Electron-phonon interactions and superconductivity in K_3C_{60}

Guanhua Chen, Yuejin Guo, Naoki Karasawa, and William A. Goddard III
Materials and Molecular Simulation Center, Beckman Institute, 139-74, Division of Chemistry and Chemical Engineering, California Institute of Technology, Pasadena, California 91125
(Received 9 July 1992; revised manuscript received 17 September 1993)

Using electronic states and phonon states from first-principles calculations on K_3C_{60} to evaluate the quantities in the McMillan equation, we examine the effects of both electron-phonon dynamic charge coupling (Q) and Jahn-Teller coupling (JT) on various superconducting properties, including T_c, ΔT_c (the shift of T_c for 1 GPa pressure), α_C (the isotope exponent for $^{12}C \rightarrow {}^{13}C$), and α_K (the isotope exponent for $^{39}K \rightarrow {}^{41}K$). All quantities including electron-phonon coupling are evaluated (without modification) directly from theory, except for the screening length between conducting electrons and ions, R_{sc}. With $R_{sc}=0.8-1.0$ Å, we find that the calculated properties, T_c, ΔT_c, and α_C, are all in good agreement with experimental measurements. We find that the superconducting properties depend critically upon the synergy between Q and JT coupling.

I. INTRODUCTION

A number of alkali-metal-doped compounds[1-3] of C_{60} (M_3C_{60}) are superconducting, with transition temperatures T_c ranging from 2.5 to 33 K. Several quite different mechanisms[4-10] have been proposed to explain the superconductivity in these materials. Zhang *et al.*[7] estimated various contributions to the electron-electron interaction in K_3C_{60} and argued that the K^+ optical-phonon modes induce a strong attraction, which is the main source of superconductivity. A suggestion by Lannoo *et al.*,[4] Johnson *et al.*,[5] and Varma, Zaanen, and Raghavachari[6] is that dynamic Jahn-Teller coupling involving high-frequency intramolecular vibrations strongly scatter electrons near the Fermi surface, leading to superconductivity. In addition to phonon-mediated electron-pairing mechanisms, Chakravarty, Gelfand, and Kivelson[8] and Baskaran and Tosatti[9] argue that two electrons may pair by electron-electron exchange and correlation on a single C_{60} molecule.

In this paper we concentrate on the role of electron-phonon interactions for the superconductivity in K_3C_{60} and consider both dynamic charge coupling (dominated by K^+ optical phonons) (Q) and Jahn-Teller (JT) coupling. We find that simultaneous inclusion of both Q and JT coupling accounts for the superconducting properties.

II. HAMILTONIAN AND ELECTRON-PHONON COUPLING

We present here a quantitative study of the superconductivity K_3C_{60} using the Hamiltonian (1)

$$H=H_{\rm ph}+H_e+H_{ee}+H^{Q}_{e\text{-ph}}+H^{\rm JT}_{e\text{-ph}} , \tag{1}$$

where each term is determined from first-principles calculations as discussed below.

A. The phonon states ($H_{\rm ph}$)

For calculating the vibrational modes of fullerene molecules, the packing of fullerenes in various crystals, and the phonon states, we developed[11] force fields in which the electrons are replaced by various two-body (bond), three-body (angle), and four-body (torsion) potentials plus long-range van der Waals interactions. These potentials were based on empirical fits to such experimental data as lattice parameters, elastic modulus, and infrared-Raman phonon states for graphite and K intercalated graphite, KC_{24}. The parameters for this force field (denoted GFF) are listed in Table I. GFF was used to predict all phonon levels for C_{60} molecules and K_3C_{60} crystal, including the pressure dependence. The vibrational frequencies for C_{60} are described quite well, as indicated in Table II (no vibrational information for C_{60} was used in determining the force field). The frequencies of IR and Raman active modes are generally predicted within 6% of the experimental values.[12] The low-frequency modes (261, 435, and 488 cm^{-1}) are calculated within about 10 cm^{-1} of the experimental measurements.[12] In comparison minimum neglected differential overlap (MNDO) quantum chemistry calculations[13] lead to an error of about 12%. We conclude that GFF gives a good description of the C_{60} vibrational modes.

We used GFF to optimize the crystal structure of K_3C_{60}. The resulting lattice constant is $A=14.18$ Å, while x-ray diffraction [14] leads to the same structure with a lattice constant[14] of 14.24 ± 0.01 Å. This force field was then used to calculate the 189 phonon modes (eigenvectors and frequencies) for each point of a $6\times6\times6$ grid in the Brillouin zone. These modes partition into (a) 174 high-frequency intramolecular bands (260 to 1520 cm^{-1}), (b) six lattice modes (130 to 140 cm^{-1}) involving tetrahedral K, (c) three lattice modes (20–50 cm^{-1}) involving octahedral K, (d) three C_{60} librational modes (30–40 cm^{-1}), and (e) three acoustic phonon modes.

Figure 1 shows the calculated distribution of phonon states for K_3C_{60}. Neutron-scattering experiment[15] on K_3C_{60} finds two broad peaks at about 35 and 120 cm^{-1}, in agreement with the calculations. We write $H_{\rm ph}$ as

$$H_{\rm ph}=\sum_{k,j}\Omega_{\mathbf{k}j}a^{\dagger}_{\mathbf{k}j}a_{\mathbf{k}j} , \tag{2}$$

TABLE I. Parameters for the graphite force field.

Interaction type[a]	Parameter[a]	GFF[b,c]
Bond stretch (Morse)	r_b (Å)	1.4114
C-C$_b$	k_b [(kcal/mol)/A^2]	720.00
	D_b (kcal/mol)	133.00
Angle bend (cosine)	θ_a (deg)	120.00
C-C-C[b]	k_θ [(kcal/mol)/rad^2]	196.13
	$k_{r\theta}$ [(kcal/mol)/rad Å]	62.709
	$k_{rr'}$ [(kcal/mol)/A^2]	68.000
Torsion (twofold)		
C-C-C-C[b]	V_t (kcal/mol)	21.280
VDW (LJ12-6)[d,e]:		
C-C[b]	$R_{v\mathrm{CC}}$ (Å)	3.8050
	$D_{v\mathrm{CC}}$ (kcal/mol)	0.0692
K-K[c]	$R_{v\mathrm{KK}}$ (Å)	4.0010
	$D_{v\mathrm{KK}}$ (kcal/mol)	0.0700
Rb-Rb[d]	$R_{v\mathrm{RbRb}}$ (Å)	4.3013
	$D_{v\mathrm{RbRb}}$ (kcal/mol)	0.0800
C-K[e]	$R_{v\mathrm{CK}}$ (Å)	3.9018
	$D_{v\mathrm{CK}}$ (kcal/mol)	0.0696
C-Rb[e]	$R_{v\mathrm{CRb}}$ (Å)	4.0455
	$D_{v\mathrm{CRb}}$ (kcal/mol)	0.0744

[a]For definitions, see S. L. Mayo, B. D. Olafson, and W. A. Goddard III, J. Phys. Chem. **94**, 8897 (1990).
[b]C parameters were optimized to fit the lattice parameters, elastic constants, and phonon frequencies for graphite.
[c]K parameters were optimized to yield the experimental geometry of KC_{24}.
[d]Rb parameters were optimized to yield the experimental geometry of RbC_{24}.
[e]R_v and D_v cross terms assumed to be geometric means.

where $\Omega_{\mathbf{k}j}$ is the frequency of mode j ($j=1$ to 189) with momentum $\mathbf{k}$.

We will be interested in the change of superconducting properties with pressure, and hence we calculated the response of the lattice parameter A to external pressure P as in Fig. 2. The calculated values fit experimental data[15,16] quite well for $P \leq 1$ GPa. Thus we calculate a change of 0.125 Å in the lattice parameter for $P=1$ GPa, while the experimental value[16] is 0.143±0.002 Å. For larger pressure, the calculated compressibility is smaller than experiment.[16] This might indicate too repulsive an inner wall in the van der Waals potential or it might indicate the effects of entrained solvent or defects in the experimental samples.

TABLE II. Vibrational frequencies (cm^{-1}) of C_{60}.

Mode	GFF	Expt.[a]	MNDO[b]
Raman			
$H_g(1)$	261	273	263
$H_g(2)$	435	434	447
$H_g(3)$	759	710	771
$H_g(4)$	750	774	924
$H_g(5)$	1080	1100	1260
$H_g(6)$	1104	1250	1407
$H_g(7)$	1321	1426	1597
$H_g(8)$	1517	1576	1722
$A_g(1)$	488	496	610
$A_g(2)$	1281	1470	1668
IR			
T_{1u} (1)	556	527	577
$T_{1u}(2)$	574	577	719
$T_{1u}(3)$	1113	1183	1353
$T_{1u}(4)$	1276	1428	1628
Abs. err	62		124

[a]Experimental results from Ref. 12.
[b]Frequencies calculated using MOPAC software (Ref. 13), also see Ref. 21.

B. The electronic states (H_e and H_{ee})

The electronic states for K_3C_{60} were calculated by Erwin and Pickett[17] using the local-density-

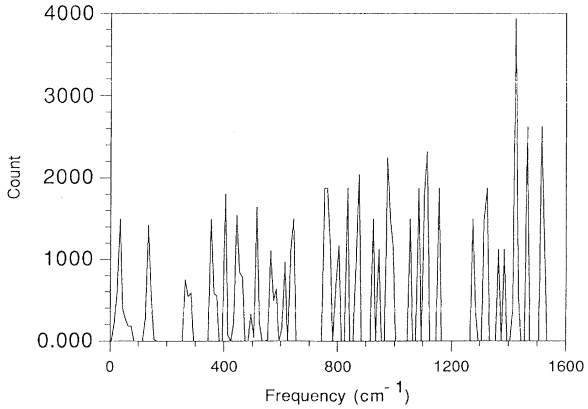

FIG. 1. Phonon density of states (arbitrary scale); the lowest two peaks below 150 cm^{-1} correspond to the intermolecular vibrations and librations and while the frequencies beyond 250 cm^{-1} correspond to C_{60} intramolecular modes.

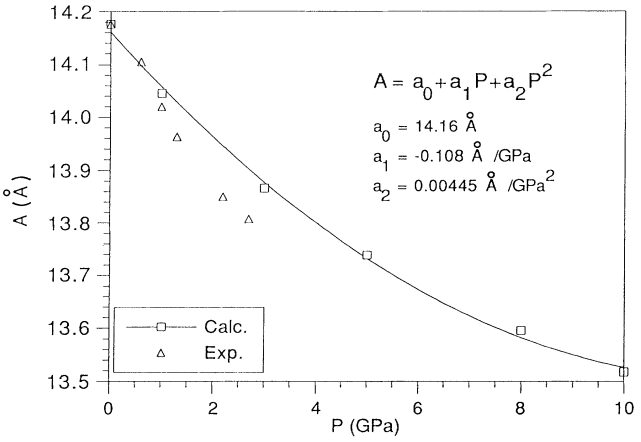

FIG. 2. Lattice constant A vs pressure P. Open squares are calculated data and open triangles are experimental data (Refs. 15 and 16). Solid line is the fit to the calculated data. We shifted our calculated data for 0 K by 0.06 Å to match with the calculated and experimental (Refs. 14–16) lattice parameter at zero pressure and 300 K.

approximation (LDA) description of the conduction bands. This led to a Fermi energy of $E_f=0.26$ eV, a conduction bandwidth of $E_w=0.6$ eV, and a density of states $N(0)=13.2$ at the Fermi energy. [The units of $N(0)$ are states per eV per C_{60} throughout the text.] In order to calculate the electronic states at 10^6 points in the Brillouin zone, we fitted the LDA results[17] to a tight-binding Hamiltonian

$$H_e=\sum_{i,j}^{\mathrm{NN}} t_{ij}^{(1)} c_{mi}^{\dagger} c_{nj}+\sum_{k}^{\mathrm{NNN}} t_{k}^{(2)} c_{mk}^{\dagger} c_{lk} \ , \tag{3}$$

including both the nearest-(NN) and the next-nearest-neighbor (NNN) hopping matrix elements. Figure 3 shows the various hopping channels including NN and NNN. For NN hoppings there are three channels with hopping matrix elements t_1, t_2, and t_3; for NNN hoppings we consider only the channel t_4 coupling two C_{60} via an intermediate K (linear configuration).

The values of t_1, t_2, t_3, and t_4 (see Fig. 4) were adjusted to fit the LDA calculation,[17] leading to a Fermi energy of $E_f=0.23$ eV and a density of states at the Fermi surface of $N(0)=11.5$. This $N(0)$ is used in all calculations unless otherwise stated. The conduction bands along $\Gamma\rightarrow X\rightarrow W\rightarrow L\rightarrow\Gamma\rightarrow K$ are plotted in Fig. 4. The density of states is given in Fig. 5.

The susceptibility and critical field[18] experiments suggest that $N(0)\approx 10-15$, while nuclear-magnetic-resonance (NMR) measurement[19] suggests $N(0)\sim 20$. An early photoemission experiment[20] reported that $N(0)=1.9$. This may be low due to the surface defects and surface sensitivity of the experiment. Our value of $N(0)$ is consistent with most of experimental results,[18,19] which suggest the range of 10–20.

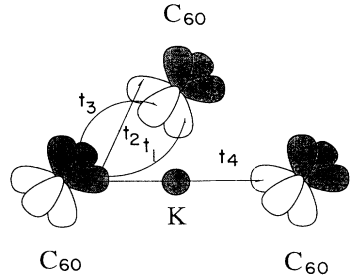

FIG. 3. Tight-binding hopping matrix elements between adjacent fullerenes. Each C_{60} molecule is represented by three p-like Gaussian orbitals with p_x and p_y are in the plane. The K atom at the octahedral site is represented by an s orbital. t_1, t_2, and t_3 are nearest-neighbor hopping matrix elements and t_4 is a next nearest neighbor hopping matrix element (through the octahedral K).

C. Dynamic charge coupling ($H_{e\text{-ph}}^{Q}$)

Dynamic charge coupling describes the changes in the electron-ion Coulomb interactions due to vibrations, assuming charges stay fixed on the ions as they vibrate. We calculated the electron-phonon coupling matrix $M_{\mathbf{k}'\mathbf{k}j}$, using the exact phonon eigenvectors and eigenenergies together with the tight-binding electronic wave functions and a local Wannier orbital representation for the conduction electrons. These Wannier orbitals were obtained by orthogonalization of Gaussian orbitals as described below.

1. Formalism

The charge coupling Hamiltonian is written as

$$H_{e\text{-ph}}^{Q}=\sum_{l}\sum_{n\alpha}\Delta\mathbf{R}_{n\alpha}\cdot\nabla_{n\alpha}V_{ei}(\mathbf{r}_l-\mathbf{R}_{n\alpha}^{(0)}) \ , \tag{4}$$

where

$$V_{ei}(r)=\exp(-r/R_{\mathrm{sc}})/r \tag{5}$$

is the screened electron-ion Coulomb interaction with a screening length R_{sc}, $\mathbf{R}_{n\alpha}^{(0)}$ is the equilibrium position of the αth ion in the nth unit cell, and $\Delta\mathbf{R}_{n\alpha}$ is its displacement,

$$\Delta\mathbf{R}_{n\alpha}=\sum_{\mathbf{k}j}\sqrt{1/NM_{\alpha}}\,Q(\mathbf{k}j)\xi(\alpha|\mathbf{k}j)\exp(i\mathbf{k}\cdot\mathbf{R}_{n\alpha}^{(0)}) \ . \tag{6}$$

Here $\xi(\alpha|\mathbf{k}j)$ is the phonon eigenvector of momentum $\mathbf{k}$ and mode j and $Q(\mathbf{k}j)$ is its amplitude.

Using the tight-binding picture, $H_{e\text{-ph}}^{Q}$ simplifies to

$$H_{e\text{-ph}}^{Q}=\frac{1}{V^{1/2}}\sum_{\mathbf{k}'\mathbf{k}j}M_{\mathbf{k}'\mathbf{k}j}c_{\mathbf{k}'}^{\dagger}c_{\mathbf{k}}(a_{-\mathbf{q}j}^{\dagger}+a_{\mathbf{q}j}) \ , \tag{7}$$

where

$$M_{\mathbf{k}'\mathbf{k}j}=-i\sum_{\mathbf{G},\alpha}\left[\frac{\hbar}{2\rho_{\alpha}\Omega_{\mathbf{q}j}}\right]^{1/2}e^{-i\mathbf{G}\cdot\mathbf{R}_{\alpha}}\hat{V}_{ei}(\mathbf{q}+\mathbf{G})\xi(\alpha|\mathbf{q}j)\cdot(\mathbf{q}+\mathbf{G})W(\mathbf{q}+\mathbf{G};\mathbf{k}',\mathbf{k}) \ . \tag{8}$$

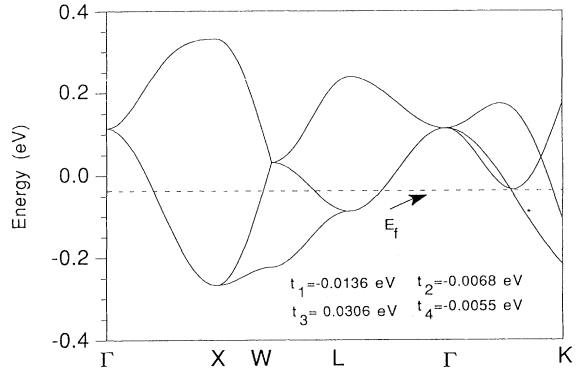

FIG. 4. The electronic bands along the $\Gamma \rightarrow X \rightarrow W \rightarrow L \rightarrow \Gamma \rightarrow K$ direction. The dashed line represents the Fermi energy.

Here

$$W(\mathbf{q}+\mathbf{G};\mathbf{k}',\mathbf{k}) = \sum_{m,n=1}^{3} A_m^*(\mathbf{k}') A_n(\mathbf{k}) U_{mn} ,$$

$$U_{mn} = \sum_{\mathrm{i}} e^{-i\mathbf{k}'\cdot\mathbf{R}_\alpha} \langle \psi_m(\mathbf{R}_\alpha) | e^{i(\mathbf{q}+\mathbf{G})\cdot\mathbf{r}} | \psi_n(0) \rangle ,$$

$\mathbf{q}=\mathbf{k}'-\mathbf{k}+\mathbf{G}$ is the first Brillouin zone, $\mathbf{G}$ is a reciprocal lattice vector, $\mathbf{A}(\mathbf{k})$ is the electronic eigenvector of momentum $\mathbf{k}$, $\mathbf{R}_\alpha$ is the equilibrium position of the αth atom in the unit cell, ψ_m is a local Wannier wave function, $\hat{V}_{ei}(\mathbf{q})=(1/V_0)V_{ei}(\mathbf{q})$, $V_{ei}(\mathbf{q})$ is the Fourier transformation of $V_{ei}(r)$ in momentum space, and V_0 is the volume of a unit cell.

All quantities in (5)–(8) were obtained directly from first-principles calculations except the screening length, R_{sc}. From Thomas-Fermi (TF) theory[21,22] the screening length is $R_{\mathrm{sc}}^{\mathrm{TF}}=\sqrt{E_f^{\mathrm{TF}}/6\pi e^2 n_e}=0.63$ Å, where $n_e=4.19\times10^{-3}$ Å^{-3} is the conduction electron density and $E_f^{\mathrm{TF}}=\hbar^2 k_f^2/2m_e=0.46$ eV is the Fermi energy of a free-electron gas model. According to the random-phase approximation[22] (RPA), the proper value for R_{sc} should be a bit larger than $R_{\mathrm{sc}}^{\mathrm{TF}}$ for interacting electron gas.

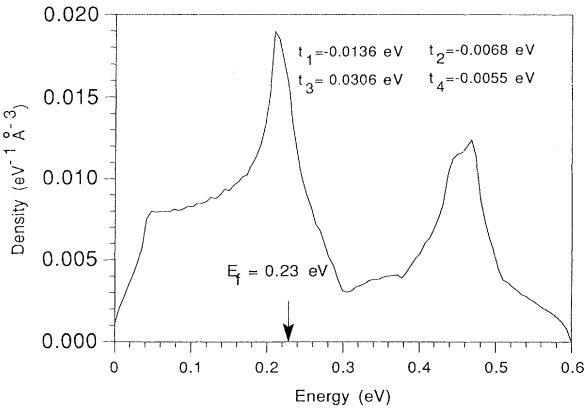

FIG. 5. Density of states for three t_{1u} bands. The arrow points at the Fermi energy.

2. Calculations

We used three p-like Gaussian functions on each C_{60} to describe the three t_{1u} orbitals and orthogonalized them up to next-nearest neighbors to obtain approximate Wannier orbitals for the three electronic bands. A typical function is $\psi_x \propto x e^{-\alpha x^2-\beta(y^2+z^2)}$, with $\alpha=0.0397$ Å^{-2} and $\beta=0.0550$ Å^{-2}. This leads to analytic expressions for all integrals. We take the charge on each K as $+e$ and on each C as $-\frac{3}{60}=-0.05e$. We determined the Fermi surface by calculating from H_e the states and energies at 1 000 000 points in the Brillouin zone, and then selected the 330 points within 0.001 eV of the Fermi energy for evaluating electron-phonon scattering matrix elements between them. The phonon eigenvectors and eigenenergies were evaluated on a $6\times6\times6$ mesh in Brillouin zone, which were used to approximate phonons at all momentum values.

3. Results

In Sec. III we summarize the McMillan formula, which relates T_c to quantities derived from the electron-phonon scattering matrix element and phonon distribution (5)–(8). A key quantity is $\alpha^2(\omega)F(\omega)$ in (13). Using the above results leads to $\alpha_Q^2(\omega)F_Q(\omega)$ for Q coupling as in Fig. 6(a). One peak at $\omega_O \approx 20$–50 cm^{-1}, involves both C_{60} librations and vibrations of K at octahedral sites. The other peak at $\omega_T \approx 130$–150 cm^{-1} involves vibrations of K at tetrahedral sites. The rest (above 200 cm^{-1}) correspond to C_{60} intramolecular vibrations and lead to negligible amplitudes. Figure 6(b) shows more detail for $\alpha_Q^2(\omega)F_Q(\omega)$ in the range from 0 to 200 cm^{-1}.

The most important quantity in superconductivity is the electron-phonon coupling constant, $\lambda=2\int\alpha^2(\omega)F(\omega)d\omega/\omega$; see (13). For Q coupling the corresponding λ_Q depends strongly on R_{sc}, increasing monotonically with R_{sc}, see Table III. λ_Q also depends on the positions and shapes of the Wannier orbitals (i.e., on the values of α and β). This is because α and β determine the relative distances between the conduction electrons and ions. There are constraints on the possible values of α and β, since the conduction electrons reside mainly on the surface of C_{60}. Contributions to λ_Q come mainly from the change in Coulomb interactions between K^+ ions and conduction electron residing on the surface of C_{60}. Because the distances between K^+ ions and the surface of C_{60} range from 3 to 11 Å, much larger than the radial variations of conduction electron density at the surface of C_{60}, we expect λ_Q to be insensitive to the detailed shape of the t_{1u} local orbitals on C_{60}. Therefore, replacing the t_{1u} orbitals by p-like Gaussian functions should be a reasonably good approximation, and we do expect the value of λ_Q to be insensitive to α and β. In addition, λ_Q is not found to be sensitive to the values of t_j ($j=1$–4).

For $R_{\mathrm{sc}}=0.63$ Å (the Thomas-Fermi value) we obtain $\lambda_Q=0.28$. For interacting electrons, according to RPA calculations[22] R_{sc} should be larger than the Thomas-Fermi length. Since the distances between the surface of

C_{60} molecules and alkali ions are about 3 Å, λ_Q is unlikely to be less than 0.28. Therefore, we conclude that electron-phonon charge coupling is too strong to be neglected in considering the mechanism of superconductivity of K_3C_{60}. This contrasts with the conclusions of some other workers.[4–6]

D. Dynamic Jahn-Teller coupling ($H_{e\text{-ph}}^{JT}$)

Lannoo *et al.*,[4] Johnson *et al.*,[5] and Varma, Zaanen, and Raghavachari[6] suggested that Jahn-Teller coupling between H_g phonon modes and t_{1u} orbitals of conduction electron might play a role in the superconductivity, and the strength of JT coupling has been estimated.[4–6] We independently calculated the Jahn-Teller coupling, obtaining coupling strengths in agreement with Ref. 6.

1. *Symmetry and electron-phonon Jahn-Teller coupling*

Calculations using both the local density approximation[23] (LDA) and MNDO (13 and 24) show that the lowest unoccupied molecular orbitals (LUMO) are of t_{1u} symmetry (p-like orbitals). According to the Jahn-Teller analysis the H_g vibrational modes (fivefold degenerate) split the degeneracy of t_{1u} states, leading to distortions of C_{60} from I_h symmetry such that the ground state is no longer degenerate. Splitting of the t_{1u} degenerate states requires that $\langle \psi_i | \partial H / \partial R_g | \psi_j \rangle$ be nonzero where ψ_i and ψ_j are components of the t_{1u} electronic states and g is a vibrational mode. This requires that the vibrational mode has a symmetry contained in the symmetric Kronecker product of t_{1u} electronic states:[25] $(t_{1u} \otimes t_{1u})_{\text{sym}} = A_g \oplus H_g$. Thus H_g vibrational modes break I_h symmetry of perfect C_{60} and split the degeneracy of three t_{1u} orbitals by inducing first-order coupling with t_{1u} electrons. This is the Jahn-Teller theorem. We examined the splitting of the t_{1u} electronic states due to all eight H_g modes.

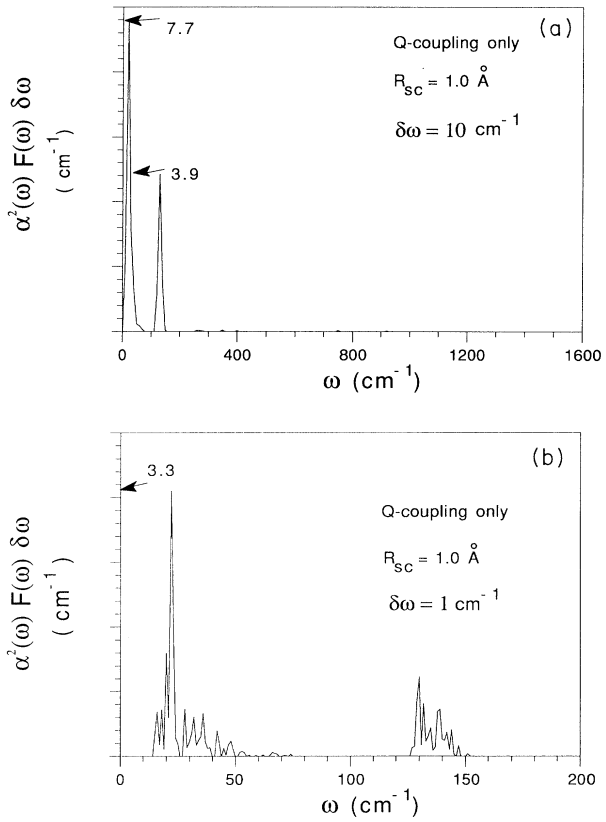

FIG. 6. $\alpha^2(\omega)F(\omega)\delta\omega$ for Q coupling. (a) ω ranges from 0 to 1600 cm^{-1}, covering the entire range of phonon modes. Data are accumulated every 10 cm^{-1}, i.e., $\delta\omega = 10$ cm^{-1}. Magnitude of the first peak (lower frequency) is 7.7 cm^{-1} and the second 3.9 cm^{-1}. (b) ω ranges from 0 to 200 cm^{-1}. Two groups of peaks correspond to coupling between conduction electron and intermolecular phonon modes. Data are accumulated every 1 cm^{-1}, i.e., $\delta\omega = 1$ cm^{-1}. The highest peak has magnitude of 3.3 cm^{-1}.

TABLE III. Values of $\lambda_Q = 2\int \alpha_Q^2(\omega) F_Q(\omega)$ as a function of screening length, R_{sc}.

R_{sc} (Å)	0.50	0.63	0.80	1.00	2.00
λ_Q	0.13	0.28	0.60	1.15	5.46

In the crystal structure[25] the oriented C_{60} molecule has T_h point-group symmetry. This splits the H_g mode into $E \oplus T$, while the t_{1u} electronic states remain degenerate. Here the E and T vibrations again lead to first-order nonzero JT-coupling matrix elements, splitting the degeneracy. Because the crystal distortions of the C_{60} molecules are very small, the coupling matrix elements in the crystal should be quite close to those of a perfect C_{60} molecule, and we have used the latter in our calculations.

2. *Formalism*

There are eight H_g modes of C_{60}, accounting for 40 of the 174 intramolecular vibration modes. The Hamiltonian for the first order couplings of the t_{1u} states has the following[6,26] form:

$$H_{ij} = \bar{E} + \sum_{m,\nu} h_{ij}(m,\nu) Q_{m,\nu} + H_{\text{vib}} , \tag{9}$$

where $i,j = 1,2,3$ are indices for the three degenerate t_{1u} electronic states, $Q_{m,\nu}$ is the normal coordinate of the mth H_g mode ($m = 1$–8) with degeneracy $\nu = 1$–5, H_{vib} is the Hamiltonian of the vibrations, $\bar{E}$ is the total energy of an undistorted C_{60}, and h_{ij} is the coefficient of the coupling matrix. For H_g modes, the coupling matrix is[6,26]

$$\frac{1}{2} g_m \begin{bmatrix} Q_{m,5} - \sqrt{3} Q_{m,4} & -\sqrt{3} Q_{m,1} & -\sqrt{3} Q_{m,2} \\ -\sqrt{3} Q_{m,1} & Q_{m,5} + \sqrt{3} Q_{m,4} & -\sqrt{3} Q_{m,3} \\ -\sqrt{3} Q_{m,2} & -\sqrt{3} Q_{m,3} & -2 Q_{m,5} \end{bmatrix} . \tag{10}$$

where g_m is the rate of energy change with respect to displacement of the mth mode. $Q_{m,5}$ is the d_z-like mode, while $Q_{m,\nu} (\nu = 1$–$4)$ are $d_{x^2-y^2}$-, d_{xy}-, d_{yz}-, and d_{zx}-like modes. For $\nu = 1$–4, the splitting from (10) is illustrated in Fig. 7(a); while for $\nu = 5$, the splitting is illustrated[6] in

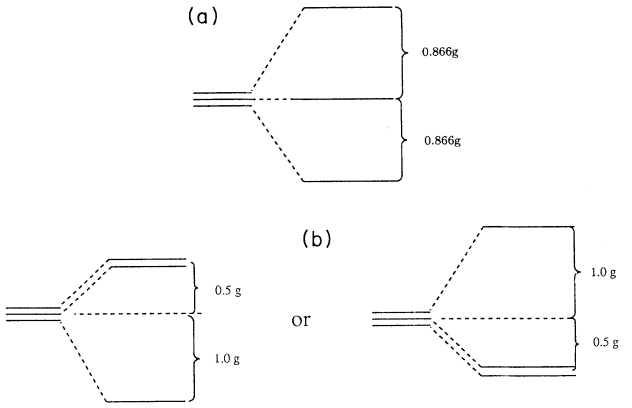

FIG. 7. (a) Energy splittings for the mode $\nu=1-4$. (b) Energy splittings for the mode $\nu=5$.

Fig. 7(b).

The dynamic Jahn-Teller electron-phonon coupling constant λ_{JT} is given by[6,26]

$$\lambda_{JT,m}=\frac{5}{6}\frac{N(0)}{M\omega_m^2}g_m^2 ,$$
$$\lambda_{JT}=\sum_m \lambda_{JT,m} . \tag{11}$$

Varma, Zaanen, and Raghavachari[6] studied the Jahn-Teller effects of a C_{60} using MNDO semiempirical quantum chemistry method[13] to calculate energies of a C_{60} molecule with frozen H_g vibrations of different amplitudes. From this they estimated the values of g_m for eight H_g vibrational modes. We used a slightly different approach to calculate the strength of JT coupling.

H_g vibrational modes split the energy degeneracy of three electronic states of t_{1u} symmetry, as illustrated in Fig. 7. The splitting is proportional to g_m. Thus, we can obtain the value of g_m for a particular H_g phonon mode, m, by measuring the splitting of the energy levels. To do this, we started with perfect C_{60} and then added frozen H_g vibrational modes from the GFF calculation [using POLYGRAF (Ref. 27)]. Finally we used MNDO (Ref. 13) to calculate the energy levels of the distorted C_{60} and from this obtained the splitting of the t_{1u} energy levels.

The total splitting is $\sqrt{3}g_m$ for $\mu=1-4$, see Fig. 7(a), and $1.5g_m$ for $\mu=5$, see Fig. 7(b). The average values for the total splittings of mode m, leads to

$$\Delta_m=1.7g_m . \tag{12}$$

3. Results

The one electron energy levels are listed in Table IV for a distortion of $Q_m=5.77\times10^{-3}$ Å ($m=1-8$), charge $Q=0$, and total spin $S=0$. The H_g modes lead to obvious splittings. Particularly, for $H_g(7)$ and $H_g(8)$, the splittings are quite large. The corresponding g_m are in reasonable agreement with the results of Ref. 6, as shown in Table V.

The result is $\lambda_{JT}=\sum_m\lambda_{JT,m}=0.75$. This compares to $\lambda_{JT}=0.64$ from Ref. 6, see Table V. Thus JT coupling is also too strong to ignore. Comparing with results of Q coupling, $\lambda_{JT}\sim\lambda_Q$ for $R_{sc}\approx0.8$ to 1.0 Å. Combining results of Q coupling and JT coupling leads to the $\lambda(\omega)$ in Fig. 8.

TABLE IV. Splittings of t_{1u} energy levels for H_g and A_g vibrational modes. The amplitudes of all phonon modes were taken as $Q_m=5.77\times10^{-3}$ Å; $m=1$ to 8 for H_g modes and 1 to 2 for A_g modes.

Mode	e_1 (eV)	e_2 (eV)	e_3 (eV)
$H_g(1)$	−2.561 29	−2.560 37	−2.559 43
$H_g(2)$	−2.560 85	−2.559 95	−2.559 28
$H_g(3)$	−2.561 12	−2.559 92	−2.558 55
$H_g(4)$	−2.562 07	−2.558 91	−2.558 36
$H_g(5)$	−2.561 06	−2.558 65	−2.558 45
$H_g(6)$	−2.560 34	−2.559 85	−2.559 17
$H_g(7)$	−2.569 62	−2.557 33	−2.552 24
$H_g(8)$	−2.566 22	−2.561 23	−2.551 60
$A_g(1)$	−2.559 03	−2.559 03	−2.559 03
$A_g(2)$	−2.546 11	−2.546 11	−2.546 11

III. CALCULATIONS OF T_c

McMillan[28] solved the Eliashberg equation numerically by a self consistent iterative procedure. He used $\alpha^2(\omega)F(\omega)$ (defined below) for Nb and calculated the T_c for several cases with different values of λ and μ^* (see Table VI for definitions). On the basis of these numerical solutions, McMillan[28] obtained an empirical formula relating the transition temperature T_c to the phonon density of states, $F_k(\omega)$, and the electron-phonon coupling matrix, $M_{k'kj}$. The McMillan formula is accurate only for $\lambda\le1.5$; however, Allen and Dynes[28] later studied cases of $\lambda\le10$. They fitted the empirical formula in (13) to the results of 217 different cases [different $\alpha^2(\omega)F(\omega)$, λ, and μ^*] leading to a rms deviation of 5.6%. Starting with

$$\alpha_{\mathbf{k}}^2(\omega)F_{\mathbf{k}}(\omega)=\frac{1}{(2\pi)^3}\sum_j\int\frac{d^2\mathbf{k}}{v_F}|M_{\mathbf{k}'\mathbf{k}j}|^2\delta(\omega-\Omega_{\mathbf{q}j}) , \tag{13a}$$

$$\alpha^2(\omega)F(\omega)=\int\frac{d^2\mathbf{k}}{v_F}\alpha_{\mathbf{k}}^2(\omega)F_{\mathbf{k}}(\omega)/\int\frac{d^2\mathbf{k}}{v_F} , \tag{13b}$$

$$\lambda=\int\lambda(\omega)d\omega=2\int\alpha^2(\omega)F(\omega)\frac{d\omega}{\omega} , \tag{13c}$$

TABLE V. Values of g_m in (10) for H_g and A_g modes. Present values are compared to those of Ref. 6. We calculated a total JT-coupling constant of $\lambda_{JT}=0.75$, which compares to $\lambda_{JT}=0.64$ of Ref. 6.

Mode	$H_g(1)$	$H_g(2)$	$H_g(3)$	$H_g(4)$	$H_g(5)$
Present	0.19	0.16	0.26	0.38	0.26
Ref. 6	0.1	0.1	0.2	0.0	0.6
Mode	$H_g(6)$	$H_g(7)$	$H_g(8)$	$A_g(1)$	$A_g(2)$
Present	0.12	1.77	1.49	0.00	0.00
Ref. 6	0.2	1.8	1.2	0	0

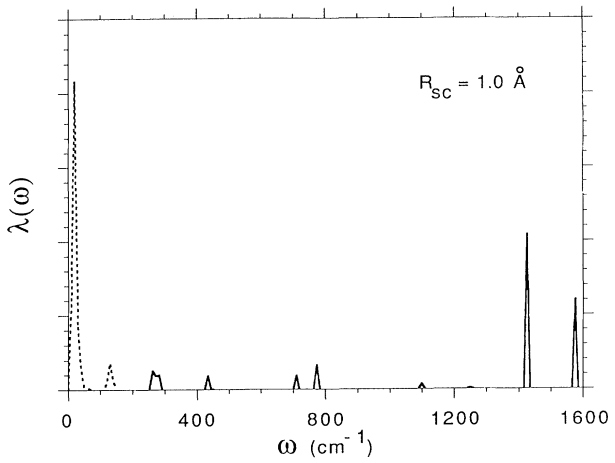

FIG. 8. Calculated values of $\lambda(\omega)=2\alpha^2(\omega)F(\omega)/\omega$ using both Q and JT coupling. Dashed line for $\lambda_Q(\omega)$ and solid line for $\lambda_{JT}(\omega)$. For $\omega<200$ cm^{-1} all contributions are from Q, while for $\omega>200$ cm^{-1} essentially all contributions are from JT. The maximum value of $\lambda(\omega)$ is 0.0669 cm.

where $v_F=(1/\hbar)\partial\epsilon_k/\partial k_\perp$ is the average Fermi velocity ($\mathbf{k}_\perp$ is perpendicular to the Fermi surface) and λ is the coupling constant, Allen and Dynes found that[28]

$$T_c=\frac{\Theta}{1.20}\exp\left[-\frac{1.04(1+\lambda)}{\lambda-\mu^*-0.62\lambda\mu^*}\right], \tag{14}$$

where various quantities are defined in Table VI.

As shown in Table VI, $\mu^*=\mu/[1+\mu\ln(E_e/\omega_{ph})]$, where E_e and ω_{ph} are the characteristic energy of conduction electron and phonon, respectively, and V_c is average screened Coulomb interaction between electrons around the Fermi surface. Following Allen and Dynes,[26] we take $\omega_{ph}=\sqrt{\langle\omega^2\rangle}$ as in Table VI. Gunnarsson and Zwicknagl[29] obtained that $\mu=0.4$. There are disagreements concerning the value of E_e. Authors of Ref. 29 used a simple two-band model to suggest that $E_e\approx 0.5E_w$. If the interband scattering matrix elements are all zero, E_e should be exactly the half of bandwidth E_w. However, E_e should be somewhat larger than $0.5E_w$. Therefore, we consider both cases $E_e=0.5E_w$ and E_w. More detailed discussion is given in Sec. V B.

IV. T_c AND OTHER PROPERTIES

Table VII shows the calculated superconducting properties for various values of R_{sc} for the cases of $E_e=0.3$ and 0.6 eV, respectively. These calculations use the density of states $N(0)=11.5$ from the tight-binding calculations. The values of μ^* for $E_e=0.6$ eV are less than those for $E_e=0.3$ eV. Therefore, the values of T_c for $E_e=0.6$ eV (15–20 K) are larger than those for $E_e=0.3$ eV (7–18 K). Given the uncertainty in the value of $N(0)$, the calculated T_c's are in a satisfactory comparison with experiments.[1–3]

The transition temperature T_c drops under external pressure,[15,16] for instance, $\Delta T_c\approx -7.2$ K for $P=1$ GPa. Using our force field we calculated directly the equilibrium structure (allowing buckling of the fullerenes) and phonons for a pressure of 1 GPa. The frequencies of the C_{60} intramolecular vibrations change less than 1%. [For instance, the frequency of $H_g(8)$ increases from 1518 to 1522 cm^{-1}.] However, for intermolecular modes the frequencies shifts are quite large, as shown in Fig. 9. The relative change is as much as 10% or more. We again calculated the phonon eigenvectors and eigenenergies from a $6\times6\times6$ grid in the Brillouin zone and recalculated the parameters in Table VI. We used $N(0)=9.2$, based on the results of a LDA calculation[23] that $N(0)$ decreases 20% under 1 GPa external pressure, and meanwhile $N(0)E_w$ was kept constant. Using these results in (13) leads to a large drop in T_c for $R_{sc}=0.5$ to 1.0 Å: $\Delta T_c=-6$ to -9 and -4 to -12 K in the cases of $E_e=0.3$ and 0.6 eV, respectively: These results are consistent with the experimental data:[16,16] $\Delta T_c\approx -7$ K.

A third significant test is the shift of T_c with isotope substitution. Experiments lead to $\alpha_C=0.30\pm0.06$ for[30] K_3C_{60} and $\alpha_C=0.37\pm0.05$ for[31] Rb_3C_{60} (an early report[32] of $\alpha_C=1.4\pm0.5$ may not be accurate). Q coupling is caused mostly by the alkali optical modes, which is affected little by the isotope substitution $^{12}C\rightarrow{}^{13}C$. To calculate the transition temperature after the isotope substitution we recalculated the eigenstates and eigenenergies of the phonon states and of $\alpha_Q^2(\omega)F_Q(\omega)$ for ^{13}C. We change only the frequencies of intramolecular modes by a scaling factor of $\sqrt{M_C/M_{13C}}$ for $\alpha^2(\omega)F(\omega)$. For $R_{sc}=0.63$ to 1.0 Å and $E_e=0.6$ eV, the resulting value of $\alpha_C\approx 0.1$, which is one-third of the experimental results.[30,31] This may be caused by breakdown of the

TABLE VI. Definitions of quantities in (14), here E_e and ω_{ph} are the characteristic energies of the conduction electrons and phonons, respectively. We take $\omega_{ph}=\sqrt{\langle\omega^2\rangle}$ and $E_e=0.5E_w$ or E_w.

$\Theta=f_1f_2\omega_{log}$	$\mu^*=\mu/[1+\mu\ln(E_e/\omega_{ph})]$
$f_1=\left[1+\left[\frac{\lambda}{\Lambda_1}\right]^{3/2}\right]^{1/3}$	$f_2=1+\frac{(\sqrt{\langle\omega^2\rangle}/\omega_{log}-1)\lambda^2}{\lambda^2+\Lambda_2^2}$
$\Lambda_1=2.46(1+3.8\mu^*)$	$\Lambda_2=1.82(1+6.3\mu^*)(\sqrt{\langle\omega^2\rangle}/\omega_{log})$
$\omega_{log}=\exp\left[\frac{2}{\lambda}\int_0^\infty\frac{d\omega}{\omega}\alpha^2(\omega)F(\omega)\ln\omega\right]$	$\langle\omega^2\rangle=\frac{2}{\lambda}\int_0^\infty d\omega\,\alpha^2(\omega)F(\omega)\omega$

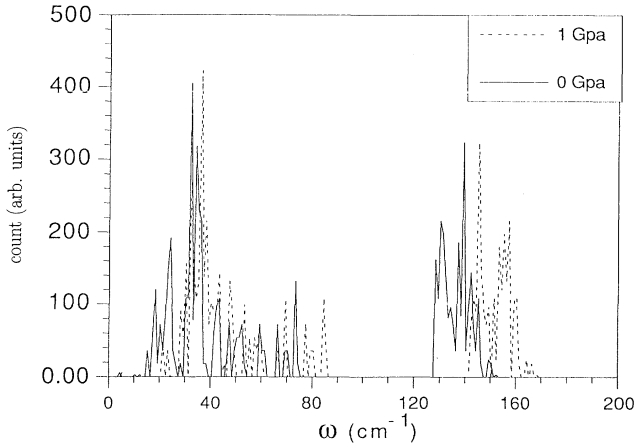

FIG. 9. Phonon distribution shifts under an external pressure of 1 GPa. The solid line is for zero external pressure, while the dashed line is for an external pressure of 1 GPa.

Eliashberg formalism. However, for $R_{sc}=2$ Å, we obtain $\alpha_C<0$, which is in clear disagreement with experiment, see Table VII.

For $^{39}K\rightarrow{}^{41}K$, we recalculated the eigenstates and eigenenergies of the phonon states and of $\alpha_Q^2(\omega)F_Q(\omega)$ after replacing ^{39}K with ^{41}K, and then recalculated T_c. The resulting values of α_K vary approximately from 0.2 to 0.3 for $R_{sc}=0.8$ to 1.0 Å, Table VII. A recent experiment[33] reports that $\alpha_{Rb}<0.2$ for Rb_3C_{60} isotope shift: $^{85}Rb\rightarrow{}^{87}Rb$.

In Table VIII we list the values of various parameters from Table VI involved in the evaluation of the transition temperature T_c.

V. FURTHER COMPARISON WITH EXPERIMENTS AND DISCUSSION

A. The value of $N(0)$

In the above calculations, $N(0)$ is fixed at the calculated value of 11.5. From experiments[18,19] $N(0)$ is believed to be in the range of 10 to 20, but the exact value of $N(0)$ is not known. In order to make more accurate comparisons of the calculated shift ΔT_c for external pressure of 1 GPa and the isotope shift α_C with experimental results, we now adjust the value of $N(0)$ to fit T_c of (14) to the experimental value,[1] as illustrated in Table IX.

After determining the value of $N(0)$ for each R_{sc}, we employed the same procedure in the previous section and calculated ΔT_c under the external pressure of 1 GPa, as indicated in Table IX. It is obvious that for $R_{sc}>1.0$ Å the values of ΔT_c are too small to account for the observed data.[16] We also calculated the isotope shifts of T_c for $^{12}C\rightarrow{}^{13}C$ (Table IX) and the resulting $\alpha_C\approx0.2$ for $E_e=E_w$, when $R_{sc}\approx0.8$–1.0 Å, which is less than experimental results[16] (again this may be due to breakdown of the Eliashberg formalism). Therefore, varying $N(0)$ to fit the observed T_c does not change the results obtained in Sec. IV.

B. The value of μ^*

The value of $\mu^*=\mu/[1+\mu\ln(E_e/\omega_{ph})]$, where E_e and ω_{ph} are the characteristic energy of conduction electron and phonon, respectively, is unknown and remains a controversial issue. The disagreement concerns the value for the characteristic electron energy, E_e. Proponents of the JT-coupling mechanism[4–6,36] argue that E_e is the size of

TABLE VII. Superconducting properties for different values of R_{sc} (the only variable in the calculations).[a] Temperature in units of K. We consider both $E_e=0.5E_w=0.3$ eV and $E_e=E_w=0.6$ eV.

E_e	R_{sc} (Å)	λ_Q/λ_{JT}	μ^*	λ	T_c	ΔT_c[a]	α_C[b]	δT_C[c]	α_K[b]	δT_K[c]
0.3 eV										
	0.50	0.2	0.31	0.9	6.8	−5.5	−0.40	0.22	0.10	−0.03
	0.63	0.4	0.30	1.1	10.5	−7.5	−0.13	0.11	0.13	−0.06
	0.08	0.8	0.29	1.4	14.2	−7.5	0.04	−0.04	0.20	−0.13
	1.00	1.5	0.28	1.9	15.5	−4.1	0.10	−0.12	0.26	−0.19
	2.00	7.3	0.24	6.2	18.3	0.7	0.02	−0.02	0.44	−0.38
0.6 eV										
	0.50	0.2	0.26	0.9	15.3	−10.1	0.05	−0.06	0.08	−0.06
	0.63	0.4	0.25	1.1	17.8	−10.1	0.12	−0.17	0.11	−0.10
	0.80	0.8	0.24	1.4	19.1	−7.3	0.15	−0.23	0.18	−0.16
	1.00	1.5	0.23	1.9	18.5	−2.8	0.15	−0.23	0.26	−0.22
	2.00	7.3	0.21	6.2	20.1	0.7	0.03	−0.04	0.45	−0.42
Expt.					19[d]	−7.2[e]	0.30(6)[f]	−0.45[f]	<0.2[g]	

[a]Change in T_c for pressure = 1 GPa = 10 kbar and A(1 GPa) = 14.04 Å.
[b]α is the isotope exponent ($T_c\propto M^{-\alpha}$). α_C for $^{12}C\rightarrow{}^{13}C$ and α_K for $^{39}K\rightarrow{}^{41}K$.
[c]Change of transition temperature upon isotope substitution.
[d]References 1–3.
[e]References 18–20.
[f]References 30–31.
[g]For Rb_3C_{60}; Ref. 33.

TABLE VIII. Parameters used in calculating T_c.

R_{sc} (Å)	ω_{log} (cm^{-1})	$\sqrt{\langle\omega\rangle}$ (cm^{-1})	f_1	f_2	Θ (cm^{-1})	μ^*	λ_Q	λ_{JT}	λ
$P=0$	$0.5E_w$								
0.50	627	1183	1.02	1.01	646	0.31	0.1	0.8	0.9
0.63	400	1094	1.03	1.01	416	0.30	0.3	0.8	1.1
0.80	215	958	1.04	1.01	226	0.29	0.6	0.8	1.4
1.00	120	811	1.07	1.02	131	0.28	1.2	0.8	1.9
2.00	42.7	452	1.36	1.16	67.4	0.24	5.5	0.8	6.2
$P=1$ GPa	$0.5E_w$								
0.50	778	1217	1.01	1.00	786	0.29	0.1	0.6	0.7
0.63	585	1156	1.02	1.01	603	0.29	0.2	0.6	0.8
0.80	375	1055	1.02	1.01	386	0.28	0.3	0.6	0.9
1.00	229	932	1.04	1.01	241	0.27	0.6	0.6	1.2
2.00	76.2	570	1.16	1.05	92.8	0.24	2.5	0.6	3.1
$P=0$	E_w								
0.50	627	1183	1.03	1.01	652	0.26	0.1	0.8	0.9
0.63	400	1094	1.03	1.01	416	0.26	0.3	0.8	1.1
0.80	215	958	1.05	1.02	230	0.24	0.6	0.8	1.4
1.00	120	811	1.08	1.02	132	0.23	1.2	0.8	1.9
2.00	42.7	452	1.39	1.19	70.6	0.21	5.5	0.8	6.2
$P=1$	E_w								
0.50	778	1217	1.02	1.00	794	0.24	0.1	0.6	0.7
0.63	585	1156	1.02	1.01	603	0.24	0.2	0.6	0.8
0.80	375	1055	1.03	1.01	390	0.24	0.3	0.6	0.9
1.00	229	932	1.04	1.01	241	0.23	0.6	0.6	1.2
2.00	76.2	570	1.17	1.06	94.5	0.21	2.5	0.6	3.1

the overall bandwidth for the molecular carbon π orbitals of C_{60}, which is about 20 eV. This leads to $\mu^* \approx 0.1$. Chakravarty, Khlebnikov, and Kivelson[37] and Gunnarsson and Zwicknagi[29] illustrated that the interband scattering between different π orbitals is much less than the intraband scattering of a π orbital for a C_{60} molecule and concluded that E_e should be the size of the conduction bandwidth E_w. In addition, Gunnarsson and Zwicknagi[29] pointed out that only the energies inside the subbands should be considered even if the interband scatter-

TABLE IX. Superconducting properties at different values of R_{sc}. The value of $N(0)$ was adjusted to yield the experimental value of T_c (19 K), while $N(0)E_w$ was kept constant. In addition to these results for $E_e=0.5E_w=0.3$ eV, we show the results for $E_e=E_w=0.6$ eV.

R_{sc} (Å)	$N(0)$ (states/eV spin C_{60})	T_c (K)[a]	λ_Q/λ_{JT}	μ^*[b]	λ	α_C[c]	ΔT_c (K)[d]	α_K[c]
			$0.5E_w$					
0.50	15.6	19.0	0.2	0.34	1.23	−0.17	−10.8	0.08
0.63	14.6	19.0	0.4	0.33	1.35	−0.04	−9.9	0.11
0.80	13.8	19.0	0.8	0.31	1.66	0.06	−6.9	0.18
1.00	14.1	19.0	1.5	0.29	2.36	0.10	−2.1	0.26
2.00	12.2	19.0	7.3	0.24	6.62	0.01	0.7	0.45
			E_w					
0.50	12.3	19.0	0.2	0.26	0.97	0.08	−11.6	0.07
0.63	11.8	19.0	0.4	0.25	1.08	0.13	−10.4	0.11
0.80	11.5	19.0	0.8	0.24	1.37	0.15	−7.3	0.18
1.00	11.8	19.0	1.5	0.23	1.98	0.16	−2.5	0.25
2.00	10.7	19.0	7.3	0.21	5.81	0.03	0.7	0.45
Expt.	10–20[e]	19[f]			0.30(6)[g]		−7.2[h]	<0.2[i]

[a]The fitted values of T_c from adjusted $N(0)$.
[b]The values of μ^* were calculated according to Table VI.
[c]Experiments: $\delta T_c(^{13}C) \approx -0.45$ K; $-\delta T_c(^{39}K) < -0.13$ K.
[d]Change of T_c when external pressure is 1 GPa, which are calculated with $N(0)(1\text{ GPa}) = 0.8N(0)(0\text{ GPa})$ [a LDA calculation (Ref. 23)] and A (1 GPa) = 14.04 Å.
[e]References 18 and 19.
[f]References 1–3.
[g]References 30 and 31.
[h]References 18–20.
[i]For Rb_3C_{60}; Ref. 33.

ings are the same magnitudes as the intraband scatterings. Therefore, considering a model in which each of sixteen subbands is 0.5 eV broad and the centers are separated by 1 eV, the effective E_e should be 1.3 eV instead of 15.25 eV (if all interband and intraband scatterings are equal). It is clear from the arguments of Ref. 37 and 29 that E_e should be in the order of the conduction bandwidth E_w. Our calculations used $E_e=0.5E_w$ and E_w. Using $\mu=0.4$ from Ref. 29, we find that $\mu^*\approx 0.2$ to 0.3, see Tables VII, VIII, and IX.

C. The energy gap

The gap-T_c ratio, $2\Delta/K_BT_c$, is an important parameter since it can be measured experimentally. Tunneling experiments[38] obtained the values of $2\Delta/K_BT_c\approx 5$ for both K_3C_{60} and Rb_3C_{60}. One far-infrared reflectivity experiment[34] concludes that $2\Delta/K_BT_c\approx 3-5$, and a recent optical reflectivity measurement[39] reports that $2\Delta/K_BT_c=3.6$ for K_3C_{60} and 2.98 for Rb_3C_{60}. Measurement of ^{13}C nuclear spin relaxation rate[19] indicates that $2\Delta/K_BT_c=3.0$ for K_3C_{60} and 4.0 for Rb_3C_{60}. Tunneling experiments indicate a strong coupling and $\lambda\approx 1.5-2.0$. Optical reflectivity and NMR data are consistent with weak coupling. Tunneling experiments may be subject to surface effects, while reflectivity and NMR measurements may indicate the minimum gap around the Fermi surface if there is a distribution of gaps. More experiments are needed for a better understanding.

For $\lambda_Q/\lambda_{JT}\leq 0.2$, we calculate $\lambda<1.0$, which is weak coupling and inconsistent with the results of tunneling experiments.[38] For $\lambda_Q/\lambda_{JT}\approx 0.4-1.5$, $\lambda\approx 1-2$, which is consistent with tunneling, optical reflection and NMR experiments. For $\lambda_Q/\lambda_{JT}\gg 1$, we calculate $\lambda\gg 1$, which is consistent only with the tunneling experiments.

The results of the tunneling experiment,[38] i.e., $2\Delta/K_BT_c\approx 5$, suggest that the magnitude of gap is $\Delta\approx 48$ K. From our tight-binding fit to LDA calculation,[17] we calculate an average velocity over the Fermi surface of $v_f=9.9\times 10^6$ cm sec^{-1}. This leads to a value of the coherence length of $\xi_0=\hbar v_f/\pi\Delta\approx 50$ Å for K_3C_{60}. The experimental result[35] is $\xi_0\approx 26$ Å. On the other hand assuming $\xi_0=26$ Å and $v_f=9.9\times 10^6$ cm sec^{-1} leads to $\Delta\approx 92$ K and the ratio $2\Delta/K_BT_c\approx 9.6$. This indicates that ξ_0 is larger than 26 Å or that v_f is less than 9.9×10^6 cm sec^{-1}. Note in Fig. 5 that the density changes very rapidly near the Fermi energy, so that v_f could conceivably be by a factor of 0.5 to 2.0.

D. Nuclear spin relaxation

^{13}C NMR measurements[19] of K_3C_{60} and Rb_3C_{60} reveal the expected linear relationship between nuclear spin relaxation rate $1/T_1$ and the temperature T in the normal state but below T_c there is an apparent suppression of the coherent peak (Hebel-Slichter peak[40]). The suppression of the Hebel-Slichter peak may indicate a broadened peak in the density of states at the edge of gap. This could be caused by a strong pairing-breaking interaction.[19,41] Using result of Ref. 41 we estimate that at $T=0.9T_c$ the enhancement of nuclear spin relaxation rate is suppressed if $\lambda\geq 2$. If $\lambda<1$ (weak-coupling superconductors), it is difficult to see how to explain the suppression of the Hebel-Slichter peak.

E. Exponent of isotope shift ($^{12}C\rightarrow{}^{13}C$)$\alpha_C$

The isotope shift yields crucial information about the mechanism of superconductivity. The exponent α_C for $^{12}C\rightarrow{}^{13}C$ is given by (15),

$$\alpha_C=-\partial\ln T_c/\partial\ln M_C \approx\frac{\lambda_{JT}}{2\lambda}\left[1-\frac{1.04(1+\lambda)(1+0.62\lambda)\mu^{*2}}{[\lambda-\mu^*(1+0.62\lambda)]^2}\right], \quad (15)$$

where M_C is the mass of carbon atom and $\lambda=\lambda_Q+\lambda_{JT}$. In the Q-coupling limit, $\lambda_{JT}\ll\lambda_Q$ and thus $\alpha_C\approx 0$. In the JT-coupling limit, $\lambda_{JT}\gg\lambda_Q$, μ^* is quite large (~ 0.3), and therefore α_C can be very small or even negative. Thus Q coupling alone can not account for the observed isotope shift[30–32] in these systems. JT coupling alone can possibly explain the observed isotope shift[30,31] only if μ^* is much less than the calculated value of ~ 0.3. For $\lambda_{JT}\sim\lambda_Q$, the calculated value of μ^* is about one third of the experimental data.[30,31] A possible explanation is that $E_e\sim\omega_{ph}$ so that the Eliashberg formalism is no longer valid.

A recent experiment on isotope effects[42] of Rb-doped C_{60} reports that the shifts of T_c 0.7, 0.5, and 0.9 K for $Rb_3{}^{13}C_{60}$, $Rb_3(^{13}C_{0.55}{}^{12}C_{0.45})_{60}$ and $Rb_3(^{13}C_{60})_{0.5}(^{12}C_{60})_{0.5}$, respectively. Our model would predict that the T_c shift of $Rb_3(^{13}C_{60})_{0.5}(^{12}C_{60})_{0.5}$ be less than that of $Rb_3{}^{13}C_{60}$. This may be caused by tight-binding approximation employed. We would like to see more experimental works.

F. Q coupling or JT coupling alone

To test whether either $H^Q_{e\text{-ph}}$ or $H^{JT}_{e\text{-ph}}$ alone can account for the superconducting properties, we carried out the same calculations using only the one coupling. In these calculations $N(0)$ is taken as the calculated value 11.5 and R_{sc} ranges from 0.5 to 2.0 Å. Table X shows that

TABLE X. Effects of not having both Q coupling and Jahn-Teller-coupling. All quantities are in the units of K.

R_{sc} (Å)	δT_c[a]	ΔT_c[b]	T_c
	Q		
0.50	*NS*[c]	*NS*[c]	*NS*[c]
0.63	0.00	*NS*[c]	~ 0
0.80	0.00	−0.6	0.6
1.00	0.00	−2.5	3.1
2.00	0.00	−3.5	15.1
	JT		
	−0.1	−8.1	11.1
Expt.	−0.45[d]	−7.2[e]	19[f]

[a] δT_c is the change for T_c upon $^{12}C\rightarrow{}^{13}C$.
[b] ΔT_c for 1 GPa pressure.
[c] NS indicates not superconducting.
[d] Reference 30.
[e] References 15 and 16.
[f] References 1–3.

$H^{Q}_{e\text{-ph}}$ alone cannot account for the superconducting properties of K_3C_{60}. Using $R_{sc}=1.0$ Å $H^{Q}_{e\text{-ph}}$ leads to $T_c \approx 3$ K, which drops for smaller R_{sc}. Larger values of R_{sc} with H^{Q}_{eph} alone leads to higher T_c (e.g., 15 K for $R_{sc}=2.0$ Å) but $\alpha_C \approx 0$ in disagreement with experiments.[30,31] Including only JT leads to $T_c \approx 11$ K, which is comparable with the observed value of 19 K. However, the very small shift of T_c upon isotope substitution $^{12}C \rightarrow {}^{13}C$ is in disagreement with experiments[30,31] (it is caused by a large value of μ^* owing to the fact that $E_e \sim \omega_{ph}$).

VI. CONCLUSION

Our conclusions are that (1) Q coupling is quite strong, and it cannot be neglected in considering the mechanism of superconductivity in K_3C_{60} and (2) the superconductivity is explained reasonably well by the Q-JT electron-phonon coupling mechanism including both $H^{Q}_{e\text{-ph}}$ and $H^{JT}_{e\text{-ph}}$.

In Sec. III C, we demonstrated that Q coupling is strong enough to play a role in the superconductivity of K_3C_{60} and cannot be neglected. The screening length should be $R_{sc} > 0.63$ Å. And hence, $\lambda_Q \geq 0.28$ and $\lambda_Q/\lambda_{JT} \geq 0.4$. However, the Q-coupling limit, $\lambda_Q/\lambda_{JT} \gg 1$, has serious problems. Because the characteristic phonon frequency is small (~ 30 cm^{-1}), it would require $\lambda > 10$ to explain the observed value of the transition temperature T_c, ~ 30 K for $Rb_{3-x}Cs_xC_{60}$,[2,3] and this would disagree with IR,[34,39] NMR,[19] and even tunneling[38] experiments. In addition, Q coupling alone cannot explain the ^{13}C isotope shift[30,31] of T_c. Therefore, Q coupling alone can be safely ruled out.

In the JT-coupling limit, $\lambda_Q/\lambda_{JT} \ll 1$, the characteristic energy of electron E_e is comparable to the characteristic energy of phonon ω_{ph}. Therefore, the effective Coulomb repulsion constant $\mu^* \approx 0.3$. This leads an isotope shift of $T_c(^{12}C \rightarrow {}^{13}C)$ of $\alpha_C \approx -0.4$ to 0.06 in disagreement with experiment.[30,31] Comparing the calculated properties and experimental results alone cannot rule out the possibility of $\lambda_{JT} \gg \lambda_Q$. However, taking into account the plausibility that $\lambda_Q \geq 0.28$, it is unlikely that these systems are in the JT coupling limit.

The calculated properties of the intermediate region, $\lambda_Q/\lambda_{JT} \sim 1$, are consistent with the current experimental observations: transition temperature[1] T_c, the shift of T_c under external pressure[15,16] ΔT_c, susceptibility[18] and NMR,[19] tunneling experiments[38] and the infrared reflection experiments.[34] That the calculated values of α_C are less than that of experimental results[30,31] may be a problem, however it could also be due to the breakdown of Eliashberg formalism or to approximations (particularly the tight-binding approximation to the LDF electronic states). Our calculations conclude that $\lambda_Q/\lambda_{JT} \approx 0.8-1.5$ (corresponding to $R_{sc}=0.8 \sim 1.0$ Å).

Our conclusion is that synergy between $H^{Q}_{e\text{-ph}}$ and $H^{JT}_{e\text{-ph}}$ leads to the special properties of bucky ball superconductors. In the range $R_{sc}=0.8$ to 1.0 Å, $\lambda_Q/\lambda_{JT} \approx 0.8-1.5$ so that both contributions are comparable. With only $H^{Q}_{e\text{-ph}}$, T_c drops substantially because λ decreases and ω_{log} becomes very small [decreasing Θ of (14)]. For only JT, λ decreases while ω_{ph} is very large, leading to a high μ^*.

Summarizing, we find that a combination of the charge and Jahn-Teller electron-phonon couplings is responsible for the superconductivity in K_3C_{60}. More definitive tests of this Q-JT mechanism will be the prediction of T_c for various mixed alkali systems[1-3] where T_c ranges from 2.5 to 33 K. There are no variables left to our disposal; thus the force fields (and hence phonons) are determined, R_{sc} must be $\sim 0.8-1.0$ Å, and the quantities in μ^* are defined. The only remaining variables have to do with the electronic states [e.g., $N(0)$ and Fermi surface], which will emerge from band calculations.

ACKNOWLEDGMENTS

We would like to thank Jean-Marc Langlois for help in the symmetry analysis and Troy Barbee III for discussions. This work was supported by NSF-CHE(90-10284) and by the Materials Simulation Center (Caltech) supported by DOE-AICD, NSF-GCAG, Allied-Signal, Asahi Glass, Asahi Chemical, BP America, Chevron, BF Goodrich, and Xerox.

[1] A. F. Hebard *et al.*, Nature (London) **350**, 600 (1991); M. J. Rosseinsky *et al.*, Phys. Rev. Lett. **66**, 2830 (1991).
[2] K. Holczer *et al.*, Science **252**, 1154 (1991).
[3] K. Tanigaki *et al.*, Nature (London) **352**, 222 (1991); **356**, 419 (1991).
[4] M. Lannoo *et al.*, Phys. Rev. B **44**, 12 106 (1991); M. Schluter *et al.*, Phys. Rev. Lett. **68**, 526 (1992).
[5] K. H. Johnson *et al.*, Physica C **183**, 319 (1991).
[6] C. M. Varma, J. Zaanen, and K. Raghavachari, Science **254**, 989 (1991).
[7] F. C. Zhang, M. Ogata, and T. M. Rice, Phys. Rev. Lett. **67**, 3452 (1991).
[8] S. Chakravarty, M. P. Gelfand, and S. Kivelson, Science **254**, 970 (1991).
[9] G. Baskaran and E. Tosatti, Current Science **61**, 33 (1991).
[10] G. Chen and W. A. Goddard III (unpublished); G. Chen, Ph.D. thesis, California Institute of Technology (1992).
[11] Y. Guo, N. Karasawa, and W. A. Goddard III, Nature (London) **351**, 464 (1991); Y. Guo, Ph.D. thesis, California Institute of Technology, 1992.
[12] D. S. Bethune *et al.*, Chem. Phys. Lett. **174**, 219 (1990); **179**, 181 (1991); T. J. Dennis *et al.*, Spectrochimica Acta **47A**, 1289 (1991); R. Meilunas *et al.*, J. Appl. Phys. **70**, 5128 (1991).
[13] M. J. S. Dewar and W. Thiel, J. Am. Chem. Soc. **99**, 4899 (1977).
[14] P. W. Stephens *et al.*, Nature (London) **351**, 632 (1991).
[15] K. Prassides *et al.*, Nature (London) **354**, 462 (1991).
[16] O. Zhou *et al.*, Science **255**, 833 (1991); G. Sparn *et al.*, **252**, 1829 (1991); R. M. Fleming *et al.*, Nature (London) **352**, 787 (1991); J. E. Schirber *et al.*, Physica C **178**, 137 (1991).
[17] S. C. Erwin and W. E. Pickett, Science **254**, 842 (1991).
[18] A. P. Ramirez *et al.*, Bull Am. Phys. Soc. **37**, 714 (1992).
[19] R. Tycko *et al.*, Science **253**, 884 (1991); R. Tycko *et al.*,

Phys. Rev. Lett. **68**, 1912 (1992).
[20]C. T. Chen *et al.*, Nature (London) **352**, 603 (1991).
[21]E. Fermi, Z. Phys. **48**, 73 (1928); L. H. Thomas, Proc. Cambridge Philos. Soc. **23**, 542 (1927); G. D. Mahan, in *Many-Particle Physics* (Plenum, New York, 1981), p. 420.
[22]D. Pines and P. Nozieres, in *The Theory of Quantum Liquids* (Addison-Wesley, Reading, MA, 1964), p. 292.
[23]S. Saito and A. Oshiyama, Phys. Rev. Lett. **66**, 2637 (1991); A. Oshiyama and S. Saito, Solid State Commun. **82**, 41 (1991).
[24]R. E. Stanton and M. D. Newton, J. Phys. Chem. **92**, 2141 (1988).
[25]F. A. Cotton, in *Chemical Applications of Group Theory* (Wiley-Interscience, New York, 1971).
[26]J. Bourgion and M. Lannoo, in *Points Defects in Semiconductors, II. Experimental Aspects,* Springer Series in Solid State Sciences, Vol. 35 (Springer-Verlag, Berlin, 1983); M. C. O'Brien, J. Phys. C **4**, 2524 (1971).
[27]These calculations were all carried out using POLYGRAF (from Molecular Simulations Inc. of Burlinton, Massachusetts) in conjunction with additional vibrational analysis software written by N. Karasawa, S. Dasgupta, and W. A. Goddard III of MSC/BI/Caltech.
[28]W. L. McMillan, Phys. Rev. **167**, 331 (1968); P. B. Allen and R. C. Dynes, Phys. Rev. B **12**, 905 (1975).
[29]O. Gunnarsson and G. Zwicknagl, Phys. Rev. Lett. **69**, 957 (1992).
[30]C.-C. Chen and C. M. Lieber, J. Am. Chem. Soc. **114**, 3141 (1992).
[31]A. P. Ramirez *et al.*, Phys. Rev. Lett. **68**, 1058 (1992).
[32]T. W. Ebbesen *et al.*, Nature (London) **355**, 620 (1992).
[33]Ebbesen *et al.*, Physica C **203**, 163 (1992).
[34]L. D. Rotter *et al.*, Nature (London) **355**, 532 (1992).
[35]K. Holczer *et al.*, Phys. Rev. Lett. **67**, 271 (1991).
[36]M. A. Schluter *et al.*, Phys. Rev. Lett. **69**, 213 (1992).
[37]S. Chakravarty, S. Khlebnikov, and S. Kivelson, Phys. Rev. Lett. **69**, 212 (1992).
[38]Z. Zheng *et al.*, Nature (London) **353**, 333 (1991); Z. Zheng and C. M. Lieber, Mod. Phys. Lett. B **5**, 1905 (1991).
[39]L. Degiorgi *et al.*, Phys. Rev. Lett. **69**, 2987 (1992).
[40]L. C. Hebel and C. P. Slichter, Phys. Rev. **113**, 1504 (1959).
[41]M. Fibich, Phys. Rev. Lett. **14**, 561 (1965).
[42]C.-C. Chen and C. M. Lieber, Science **259**, 655 (1993).